

## ***Supporting Information***

### **Polyoxometalates Covalent Combined with Graphitic Carbon Nitride for Photocatalytic Hydrogen Peroxide Production**

*Shen Zhao,<sup>a</sup> Xu Zhao,<sup>\*a,b</sup> Shuxin Ouyang,<sup>c,d,e</sup> Yongfa Zhu<sup>f</sup>*

<sup>a</sup>Key Laboratory of Drinking Water Science and Technology, Research Center for Eco-Environmental Sciences, Chinese Academy of Sciences, Beijing, 100085, China

<sup>b</sup>University of Chinese Academy of Sciences, Beijing, 100049, China

<sup>c</sup>TU-NIMS Joint Research Center, School of Materials Science and Engineering, Tianjin University, Tianjin, 300072, China

<sup>d</sup>Collaborative Innovation Center of Chemical Science and Engineering (Tianjin), Tianjin 300072, China

<sup>e</sup>Key Lab of Advanced Ceramics and Machining Technology, Ministry of Education, Tianjin 300072, China

<sup>f</sup>Department of Chemistry, Tsinghua University, Beijing, 100084, China

#### **List of contents**

##### **Experimental Section**

**Figure S1.** CO<sub>2</sub>-TPD profiles (A) and photocatalytic H<sub>2</sub>O<sub>2</sub> production (B) of 3DOM g-C<sub>3</sub>N<sub>4</sub> and g-C<sub>3</sub>N<sub>4</sub>.

**Figure S2.** Preparation process of g-C<sub>3</sub>N<sub>4</sub>-SiW<sub>11</sub>.

**Figure S3.** XRD patterns of g-C<sub>3</sub>N<sub>4</sub>, K-SiW<sub>11</sub> and g-C<sub>3</sub>N<sub>4</sub>-SiW<sub>11</sub>.

**Figure S4.** IR spectra of g-C<sub>3</sub>N<sub>4</sub>, K-SiW<sub>11</sub> and g-C<sub>3</sub>N<sub>4</sub>-SiW<sub>11</sub>.

**Figure S5.** CO<sub>2</sub>-TPD profiles of g-C<sub>3</sub>N<sub>4</sub> and g-C<sub>3</sub>N<sub>4</sub>-SiW<sub>11</sub>.

**Figure S6.** Zeta potentials of g-C<sub>3</sub>N<sub>4</sub> and g-C<sub>3</sub>N<sub>4</sub>-SiW<sub>11</sub>.

**Figure S7.** Adsorption-desorption isotherms (A) and pore size distribution curves (B) of g-C<sub>3</sub>N<sub>4</sub> and g-C<sub>3</sub>N<sub>4</sub>-SiW<sub>11</sub>.

**Figure S8.** TGA curves for g-C<sub>3</sub>N<sub>4</sub>, K-SiW<sub>11</sub>, and g-C<sub>3</sub>N<sub>4</sub>-SiW<sub>11</sub>.

**Figure S9.** TEM images of g-C<sub>3</sub>N<sub>4</sub> (A-C) and g-C<sub>3</sub>N<sub>4</sub>-SiW<sub>11</sub> (D-F).

**Figure S10.** STEM images (A and B) and corresponding elemental mappings (C-G) of g-C<sub>3</sub>N<sub>4</sub>-SiW<sub>11</sub>.

**Figure S11.** Photocatalytic H<sub>2</sub>O<sub>2</sub> production over g-C<sub>3</sub>N<sub>4</sub>-SiW<sub>11</sub> in the presence of different electron donors.

**Figure S12.** Photocatalytic H<sub>2</sub>O<sub>2</sub> production over g-C<sub>3</sub>N<sub>4</sub> and g-C<sub>3</sub>N<sub>4</sub>-SiW<sub>11</sub> under N<sub>2</sub>- and O<sub>2</sub>-equilibrated conditions.

**Figure S13.** Photocatalytic H<sub>2</sub>O<sub>2</sub> production over g-C<sub>3</sub>N<sub>4</sub> and g-C<sub>3</sub>N<sub>4</sub>-SiW<sub>11</sub> under visible light ( $\lambda > 400$  nm) and sunlight (AM 1.5 filter).

**Figure S14.** Photocatalytic H<sub>2</sub>O<sub>2</sub> decomposition over different catalysts.

**Figure S15.** <sup>13</sup>C (A) and <sup>29</sup>Si (B) MAS NMR spectra of fresh and used g-C<sub>3</sub>N<sub>4</sub>-SiW<sub>11</sub>.

**Figure S16.** Photocatalytic H<sub>2</sub>O<sub>2</sub> production over 3DOM g-C<sub>3</sub>N<sub>4</sub>-PW<sub>11</sub> and g-C<sub>3</sub>N<sub>4</sub>-SiW<sub>11</sub> in the presence of methanol.

**Figure S17.** LSV curves of catalysts-loaded electrodes toward OER with scan rate of 10 mV·s<sup>-1</sup> in the dark.

**Figure S18.** Photocurrent response of catalysts-loaded electrodes under sunlight (AM 1.5 filter) at a bias of 0.25 V vs. SCE (A); EIS Nyquist plots of the catalysts under sunlight (AM 1.5 filter) at a bias of 5 mV vs. SCE in the frequency range of 10 mHz to 100 kHz (B).

**Figure S19.** PL spectra (A), UV-DRS spectra (B), and Tauc plots of g-C<sub>3</sub>N<sub>4</sub> and g-C<sub>3</sub>N<sub>4</sub>-SiW<sub>11</sub>.

**Figure S20.** NBT decomposition (A) and •OOH radicals formation (B) during the photoreaction over g-C<sub>3</sub>N<sub>4</sub> and g-C<sub>3</sub>N<sub>4</sub>-SiW<sub>11</sub>.

**Figure S21.** The effect of PBQ for the photocatalytic H<sub>2</sub>O<sub>2</sub> production over g-C<sub>3</sub>N<sub>4</sub> and g-C<sub>3</sub>N<sub>4</sub>-SiW<sub>11</sub>.

**Figure S22.** LSV curves of g-C<sub>3</sub>N<sub>4</sub> (A), TBA-SiW<sub>11</sub> (B) and g-C<sub>3</sub>N<sub>4</sub>-SiW<sub>11</sub> (C) measured on RDE analysis at different rotating speeds.

**Figure S23.** Mott-Schottky plots of g-C<sub>3</sub>N<sub>4</sub> (A) and g-C<sub>3</sub>N<sub>4</sub>-SiW<sub>11</sub> (B) with frequency of 1.0 kHz, 1.5 kHz, and 2.0 kHz in the dark.

**Figure S24.** Experiment to prove the heterogeneous nature (A) and the recycle (B) of g-C<sub>3</sub>N<sub>4</sub>-SiW<sub>11</sub>.

**Figure S25.** XRD patterns (A) and IR spectra (B) of fresh and used g-C<sub>3</sub>N<sub>4</sub>-SiW<sub>11</sub>.

**Figure S26.** STEM images and corresponding elemental mappings of used g-C<sub>3</sub>N<sub>4</sub>-SiW<sub>11</sub>.

**Table S1.** Porous structural parameter for g-C<sub>3</sub>N<sub>4</sub> and g-C<sub>3</sub>N<sub>4</sub>-SiW<sub>11</sub>.

**Table S2.** ICP and EA analysis of g-C<sub>3</sub>N<sub>4</sub> and g-C<sub>3</sub>N<sub>4</sub>-SiW<sub>11</sub>.

**Table S3.** Products distribution for photocatalytic H<sub>2</sub>O<sub>2</sub> production over different catalysts in 60 minutes.

**Table S4.** Rate constants for photocatalytic H<sub>2</sub>O<sub>2</sub> formation and decomposition over different catalysts.

**Table S5.** Cartesian coordinates for the models for SiW<sub>11</sub>-organic linker.

**Table S6.** Cartesian coordinates for the models for g-C<sub>3</sub>N<sub>4</sub>-SiW<sub>11</sub>.

**Table S7.** Mulliken charge distribution on O atoms of SiW<sub>11</sub>-organic linker and g-C<sub>3</sub>N<sub>4</sub>-SiW<sub>11</sub> by DFT method.

**References**

## Experimental Section

**Chemicals:** urea, (triethoxysilyl)-propyl isocyanate, triethylamine, nitro blue tetrazolium (NBT) and *p*-benzoquinone (PBQ) were purchased from Alfa Aesar company and used as received without further purification. 5,5-dimethyl-1-pyrroline (DMPO) were purchased from Sigma-Aldrich company. All solvents used were of analytical grade and were purchased from Fisher.  $K_8[SiW_{11}O_{39}] \cdot 13H_2O$  (K-SiW<sub>11</sub>)<sup>S1</sup> were synthesized and characterized in accordance with the literature.

**Measurements:** The powder X-ray diffraction (XRD) patterns were measured on an X-ray diffractometer (X'Pert PRO MPD) equipped with a Cu K $\alpha$  radiation source ( $\lambda = 0.15405$  nm, 40 kV and 40 mA). Fourier transform infrared (FTIR) spectroscopy measurements were performed applying a Nicolet 5700 spectrometer under ambient air (40 scans at a resolution of 4 cm<sup>-1</sup>) in attenuated total reflectance (ATR) mode. The N<sub>2</sub> adsorption-desorption experiments were performed on a Micromeritics ASAP 2020 instrument at liquid N<sub>2</sub> temperature (-196 °C). The samples were outgassed at 110 °C for 6 hours prior to N<sub>2</sub> adsorption. Thermogravimetric analysis (TGA) was performed on a TGA/DSC 1 STARe from Mettler Toledo in flowing air from 50 °C to 800 °C with a heating rate of 10 °C/min. Temperature programmed desorption (TPD) of CO<sub>2</sub> and O<sub>2</sub> were measured with a Micromeritics ChemiSorb 2720 chemisorption analyzer. For CO<sub>2</sub>-TPD, after pretreated at 300 °C in He for 1 hour, the samples were first purged under 40% CO<sub>2</sub> for 1 hour, and then isothermally removed physical adsorbed CO<sub>2</sub> in He for 30 minutes. The TPD measurement was carried out in He at a rate of 10 °C/min up to 400 °C. The gas flow rate was 50 ml/min. In the case of O<sub>2</sub>-TPD, after pretreated at 300 °C in He for 1 hour, the samples were first purged under 5% O<sub>2</sub> for 1 hour, and then isothermally removed physical adsorbed O<sub>2</sub> in He for 30 minutes. The TPD measurement was carried out in He at a rate of 10 °C/min up to 500 °C. The gas flow rate was 50 ml/min. Zeta potential measurements were performed using a Zetasizer Nano ZS (Malvern Instruments) based on dynamic light-scattering analysis. Inductively coupled plasma-atomic emission spectroscopy (ICP-AES) analysis was performed on a Shimadzu ICPS-7500 instrument. The elemental analysis (EA) was performed on an EAI CE-440 elemental analyzer. Solid state NMR measurements were carried out on a Bruker Avance 300 M solid-state

spectrometer equipped with a commercial 5 mm MAS NMR probe. The X-ray photoelectrospectroscopy (XPS) was measured using a Phi Quantern instrument. The binding energies were calibrated with C 1s=284.8 eV. Transmission electron microscopy (TEM) images were recorded on a JEM-2011 instrument at a voltage of 200 kV. The samples were prepared by ultrasonic dispersion in ethanol and dispersed for several minutes, and the transparent suspended droplets were placed on a copper grid using a capillary. UV-vis diffuse reflection spectra (DRS) were obtained on a Hitachi U-3010 UV-vis spectrophotometer. BaSO<sub>4</sub> was used as the reflectance standard in the experiment. The room-temperature photoluminescence (PL) spectra of TCN were recorded on Perkin-Elmer LS55 spectrophotometer with an excitation wavelength of 388 nm. To calculate the apparent quantum yield (AQY), the incident light was passed through a SAP301 grating monochromator (Newport, Oriel 77250). The light intensity was measured using an optical power meter (1815-C, Newport) with a photodiode detector (818-UV, Newport). The light intensities at 320, 370, 420, 470, and 520nm were measured as 0.16, 0.40, 0.74, 1.06, and 0.75 mW, respectively. AQY was estimated from the formula  $\Phi_{AQY} (\%) = ((\text{number of H}_2\text{O}_2 \text{ molecules formed}) \times 2) / (\text{number of incident photons}) \times 100$ .

**Preparation of g-C<sub>3</sub>N<sub>4</sub>:**<sup>S2</sup> g-C<sub>3</sub>N<sub>4</sub> was prepared by thermally decomposing urea at 550 °C in a crucible with a cover for 4 hours in static air with a ramp rate of 3 °C·min<sup>-1</sup>. Then, the crucible was cooled to room temperature naturally. The resulting yellow product was collected and ground into fine powder for further use. Based on the TGA and EA analysis, the formula of g-C<sub>3</sub>N<sub>4</sub> was determined to be C<sub>2.61</sub>N<sub>4</sub>H<sub>1.58</sub>.

**Photoelectrochemical measurements:** The photoelectrochemical measurements were performed using a three-electrode cell connected to an electrochemical CHI 660 B workstation (Shanghai, China). The saturated calomel electrode (SCE) and Pt wire (70 mm in length with a 0.4-mm diameter) were used as reference and counter electrode, respectively. The working electrode was fabricated by immobilizing catalysts on the FTO conductive glass by a casting method. The as-prepared catalysts (10 mg) were dispersed in a solution (ethanol: 800 μl, Nafion: 200 μl), and sonicated for 3 hours. Subsequently, the resultant suspension was cast dropwise on the surface of the FTO. The FTO electrodes immobilized with the samples were connected to a copper tape and used as the working electrode. The working electrode was irradiated with light obtained from a 300 W Xe lamp (Perfect Light company, Beijing) and used the AM 1.5 filter to

simulate the sunlight. Chopped-light amperometric *I-t* characterizations were evaluated at an applied potential of 0.25 V vs. SCE under chopped light irradiation (light on or off cycles: 30 s). Electrochemical impedance spectroscopy (EIS) was conducted by applying a AC voltage amplitude of 5 mV vs. SCE within the frequency range from  $10^5$  to 0.01 Hz with 0.05 M  $\text{Na}_2\text{SO}_4$  solution under the open-circuit potential (OCP) and sunlight irradiation (AM 1.5 filter). The linear sweep voltammogram (LSV) measurements were obtained in 0.05 M  $\text{Na}_2\text{SO}_4$  solution at 25 °C at a scan rate of  $10 \text{ mV}\cdot\text{s}^{-1}$  in the dark. Mott-Schottky plots were measured in 0.05 M  $\text{Na}_2\text{SO}_4$  solution at a frequency of 1 kHz in the dark. The potentials measured were converted to normal hydrogen electrode (NHE) based on the Eqn. S1:

$$E(\text{NHE}) = E(\text{SCE}) + 0.24 \quad (\text{Eqn. S1})$$

**Rotating Disk Electrode (RDE) Measurements:** The measurements were performed on a Pine AFMSRXE 1523 advanced electrochemical system with a three-electrode cell using an Ag/AgCl electrode and a Pt wire electrode as the reference and counter electrode, respectively.<sup>S3</sup> The working electrode was prepared as follows: catalysts (50 mg) were dispersed in EtOH (2 ml) containing Nafion (50 mg) by ultrasonication. The slurry (20  $\mu\text{l}$ ) was put onto a Pt disk electrode and dried at room temperature. The LSV were obtained in an  $\text{O}_2$ -saturated 0.1 M phosphate buffer solution (pH 7) with a scan rate  $10 \text{ mV}\cdot\text{s}^{-1}$  after  $\text{O}_2$  bubbling for 5 min. The average number of electrons (*n*) involved in the overall  $\text{O}_2$  reduction can be estimated by the linear regression of the plots using the following equations:

$$j^{-1} = j_k^{-1} + B^{-1}\omega^{-1/2} \quad (\text{Eqn. S2})$$

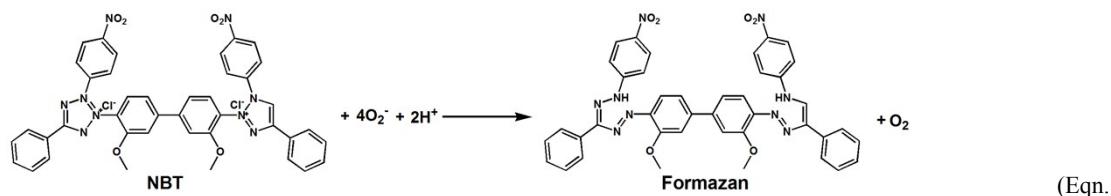
$$B = 0.2nF\nu^{-1/6}CD^{2/3} \quad (\text{Eqn. S3})$$

*j* is the current density, *j<sub>k</sub>* is the kinetic current density,  $\omega$  is the rotating speed (rpm), *F* is the Faraday constant ( $96485 \text{ C}\cdot\text{mol}^{-1}$ ),  $\nu$  is the kinetic viscosity of water ( $0.01 \text{ cm}^2\cdot\text{s}^{-1}$ ), *C* is the bulk concentration of  $\text{O}_2$  in water ( $1.26 \times 10^{-3} \text{ mol}\cdot\text{cm}^{-3}$ ), and *D* is the diffusion coefficient of  $\text{O}_2$  ( $2.7 \times 10^{-5} \text{ cm}^2\cdot\text{s}^{-1}$ ), respectively.<sup>S4</sup>

**•OOH radical examination:** •OOH was examined by a Bruker model electron spin resonance (ESR) A300-10/12 spectrometer equipped with a quanta-Ray Nd: YAG laser system employing 5,5-dimethyl-1-pyrroline-N-oxide (DMPO) as the spin trapper. Typically, catalyst (0.10 g) was added to a methanol/water mixture (9/1 v/v, 100 ml) containing DMPO (0.125 mmol) within a container. After  $\text{O}_2$  bubbling for 10 minutes, the container was photo irradiated for 3 minutes. The

catalyst was recovered by filtration, and the solution was subjected to analysis at room temperature.

**Quantitative experiment of  $\bullet\text{OOH}$ :**<sup>S5</sup> In order to quantify the  $\bullet\text{OOH}$  concentration, nitro blue tetrazolium (NBT) has been chosen as a  $\bullet\text{OOH}$  radical scavenger because NBT can be reduced by  $\bullet\text{OOH}$  radicals and formed purple formazan, which was insoluble in water. The photocatalytic activities were evaluated by the activation of oxygen under sunlight irradiation (AM 1.5 filter). A 300 W Xenon lamp (Perfect Light Company, Beijing) was chosen as light source. During each photocatalytic performance, 0.10 g of catalyst was added to a methanol/water mixture (5/95 v/v, 100 ml) containing NBT (0.02 mM) within a container (1 g·L<sup>-1</sup> catalyst). After that, the dispersion was stirred in the dark for 60 minutes to ensure the adsorption-desorption equilibrium among the catalyst, dissolved oxygen and water before light irradiation. During the irradiation, 3.0 ml of the suspensions was taken from the reaction cell at given time intervals, and then filtrated to remove the catalysts. The concentration of  $\bullet\text{OOH}$  radicals was determined by the degradation of NBT, measured by the absorbance change at the wavelength of 259 nm. The mole ratio of generated  $\bullet\text{OOH}$  radicals and degraded NBT was 4: 1 according to the following equation:



**Calculation Details:** Density functional theory (DFT)<sup>S6</sup> with B3LYP<sup>S7</sup> was used to optimize the geometries of complexes 1 and 2. In all calculations, a 'double- $\xi$ ' quality basis set LANL2DZ<sup>S8</sup> was employed on W atom, and 6-31G(d) basis set was used for other atoms in the optimizations. There were no symmetry constraints on these complexes. All calculations were performed with Gaussian 09 software package of programs.<sup>S9</sup> Cartesian coordinates for the models used are summarized in Table S4 and S5.

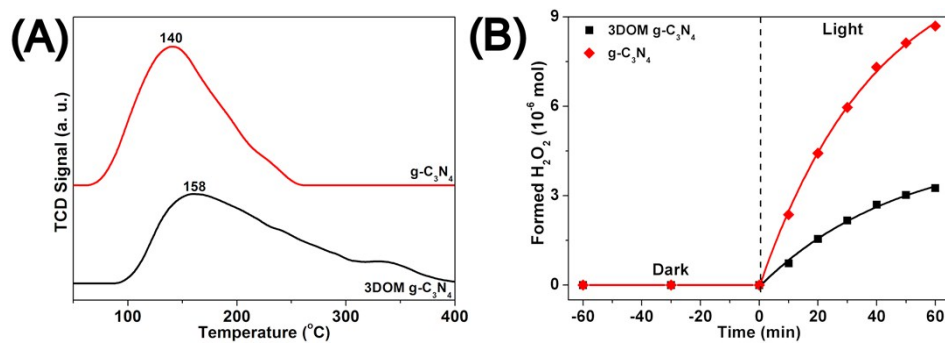


**Figure S1.** CO<sub>2</sub>-TPD profiles (A) and photocatalytic H<sub>2</sub>O<sub>2</sub> production (B) of 3DOM g-C<sub>3</sub>N<sub>4</sub> and g-C<sub>3</sub>N<sub>4</sub>. Reaction conditions: methanol/water mixture (5/95 v/v, 100 ml), catalyst (0.10 g, 1 g·L<sup>-1</sup>), O<sub>2</sub>-equilibrated, AM 1.5 filter, 25 °C.

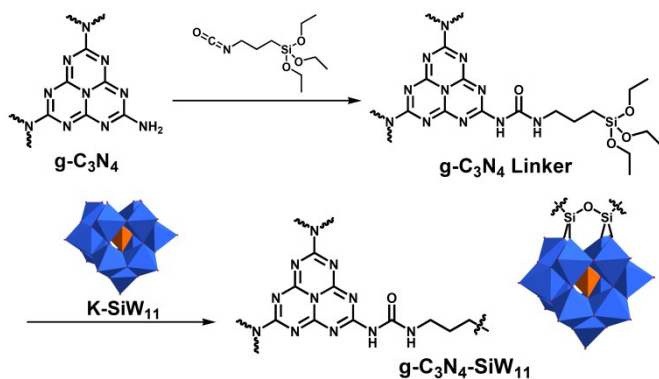


**Figure S2.** Preparation process of g-C<sub>3</sub>N<sub>4</sub>-SiW<sub>11</sub>.

As shown in Fig. S2, the organosilicon linkers can be grafted onto g-C<sub>3</sub>N<sub>4</sub> through the formation of carbamido groups to generate the g-C<sub>3</sub>N<sub>4</sub> linker. The POM cluster of SiW<sub>11</sub> can covalently connect with g-C<sub>3</sub>N<sub>4</sub> linker under acidic solution. In this way, the POM cluster of SiW<sub>11</sub> has been covalently combined with g-C<sub>3</sub>N<sub>4</sub> to form the hybrid catalyst of g-C<sub>3</sub>N<sub>4</sub>-SiW<sub>11</sub> for photocatalytic H<sub>2</sub>O<sub>2</sub> production.

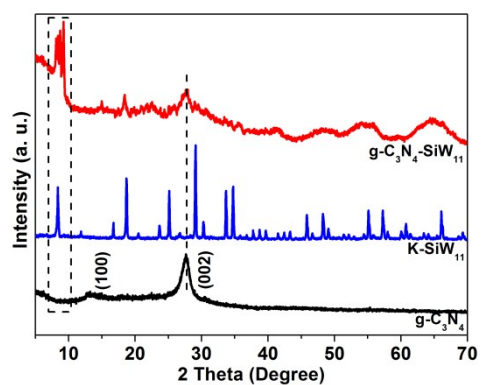


Figure S3. XRD pattern of  $g\text{-C}_3\text{N}_4$ ,  $\text{K-SiW}_{11}$  and  $g\text{-C}_3\text{N}_4\text{-SiW}_{11}$ .

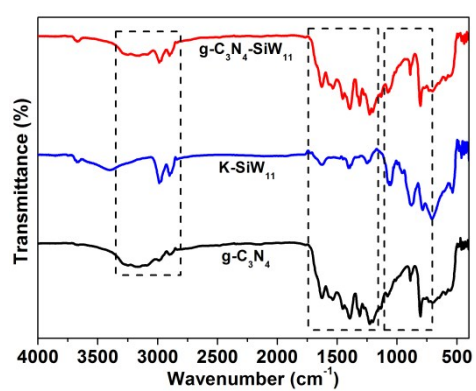


Figure S4. IR spectra of  $g\text{-C}_3\text{N}_4$ ,  $\text{K-SiW}_{11}$  and  $g\text{-C}_3\text{N}_4\text{-SiW}_{11}$ .

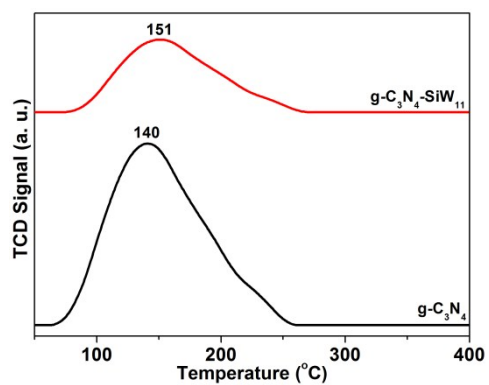


Figure S5.  $\text{CO}_2$ -TPD profiles of  $g\text{-C}_3\text{N}_4$  and  $g\text{-C}_3\text{N}_4\text{-SiW}_{11}$ .

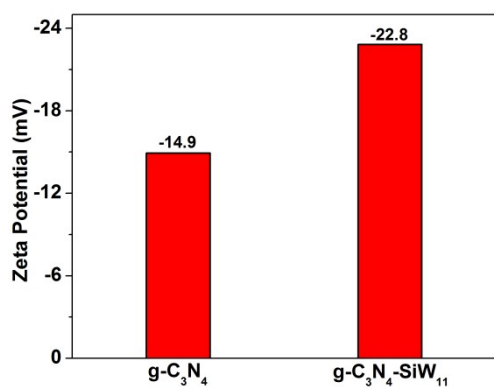


Figure S6. Zeta potentials of g-C<sub>3</sub>N<sub>4</sub> and g-C<sub>3</sub>N<sub>4</sub>-SiW<sub>11</sub>.

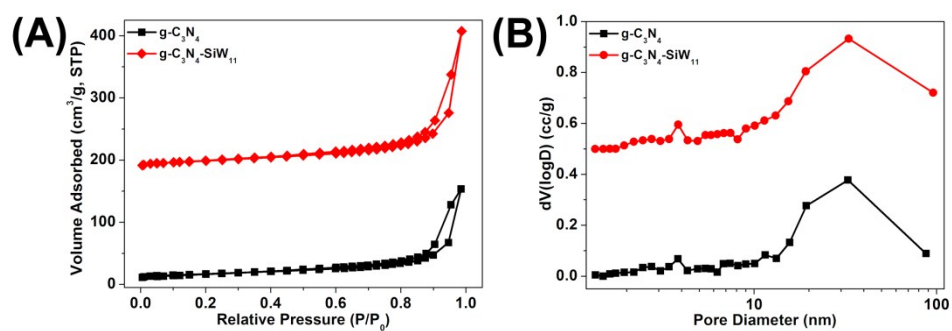


Figure S7. Adsorption-desorption isotherms (A) and pore size distribution curves (B) of g-C<sub>3</sub>N<sub>4</sub> and g-C<sub>3</sub>N<sub>4</sub>-SiW<sub>11</sub>.

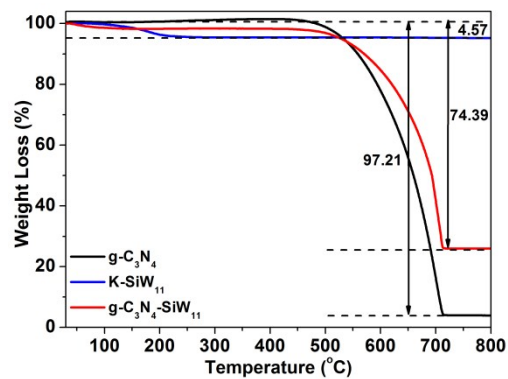
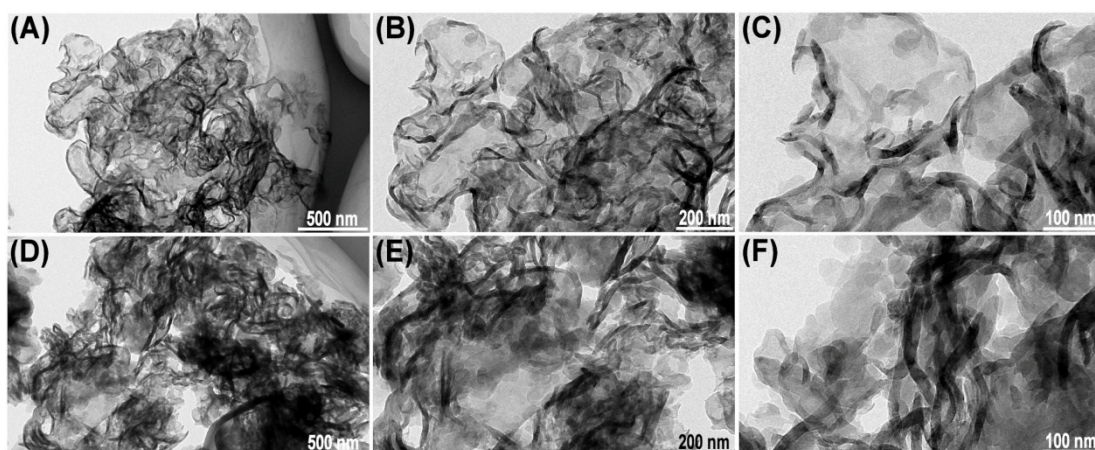
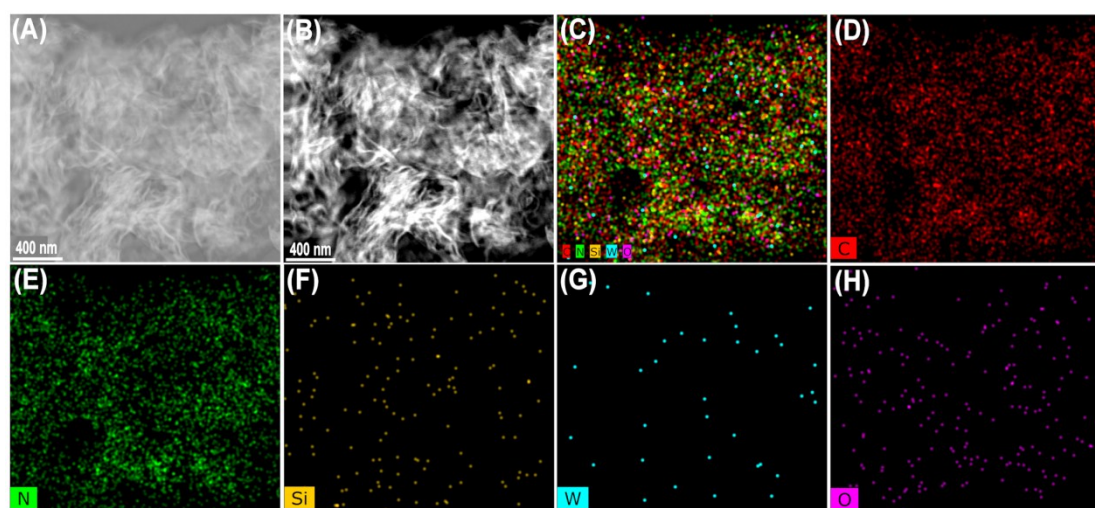


Figure S8. TGA curves for g-C<sub>3</sub>N<sub>4</sub> (A), K-SiW<sub>11</sub> (B), and g-C<sub>3</sub>N<sub>4</sub>-SiW<sub>11</sub> (C).



**Figure S9.** TEM images of g-C<sub>3</sub>N<sub>4</sub> (A-C) and g-C<sub>3</sub>N<sub>4</sub>-SiW<sub>11</sub> (D-F).



**Figure S10.** STEM images (A and B) and corresponding elemental mappings (C-G) of g-C<sub>3</sub>N<sub>4</sub>-SiW<sub>11</sub>.

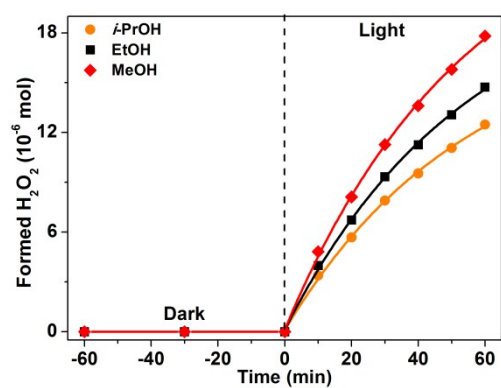


**Figure S11.** Photocatalytic H<sub>2</sub>O<sub>2</sub> production over g-C<sub>3</sub>N<sub>4</sub>-SiW<sub>11</sub> in the presence of different electron donors. Reaction conditions: alcohol (methanol, ethanol and *i*-propanol)/water mixture (5/95 v/v, 100 ml), catalyst (0.10 g, 1 g·L<sup>-1</sup>), O<sub>2</sub>-equilibrated, AM 1.5 filter, 25 °C.

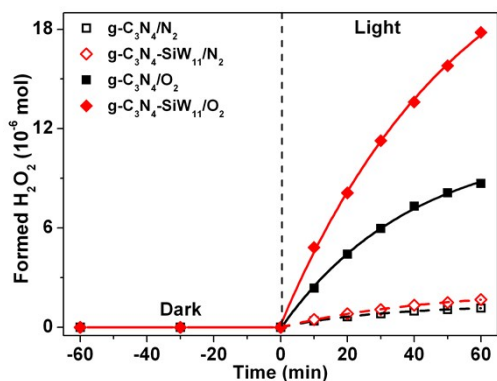


**Figure S12.** Photocatalytic H<sub>2</sub>O<sub>2</sub> production over g-C<sub>3</sub>N<sub>4</sub> and g-C<sub>3</sub>N<sub>4</sub>-SiW<sub>11</sub> under N<sub>2</sub>- and O<sub>2</sub>-equilibrated conditions. Reaction conditions: methanol/water mixture (5/95 v/v, 100 ml), catalyst (0.10 g, 1 g·L<sup>-1</sup>), N<sub>2</sub> or O<sub>2</sub>-equilibrated, AM 1.5 filter, 25 °C.

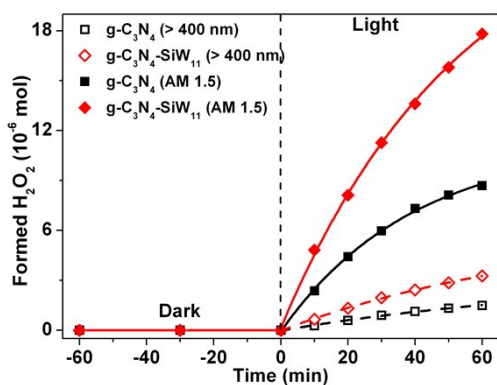


**Figure S13.** Photocatalytic H<sub>2</sub>O<sub>2</sub> production over g-C<sub>3</sub>N<sub>4</sub> and g-C<sub>3</sub>N<sub>4</sub>-SiW<sub>11</sub> under visible light ( $\lambda > 400$  nm) and sunlight (AM 1.5 filter). Reaction conditions: methanol/water mixture (5/95 v/v, 100 ml), catalyst (0.10 g, 1 g·L<sup>-1</sup>), O<sub>2</sub>-equilibrated,  $\lambda > 400$  nm or AM 1.5 filter, 25 °C.

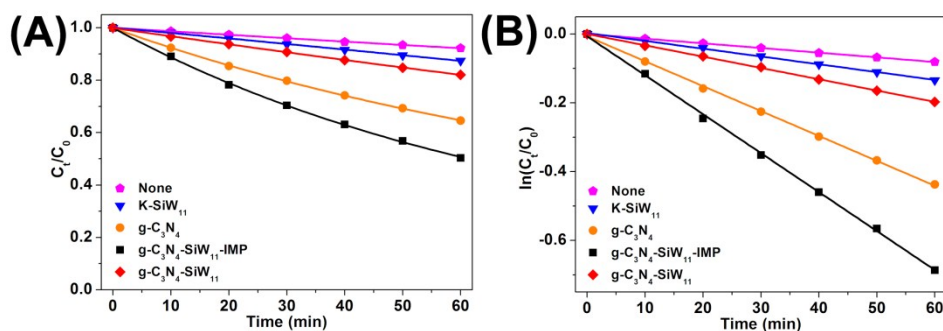


**Figure S14.** Photocatalytic H<sub>2</sub>O<sub>2</sub> decomposition over different catalysts. Reaction conditions: H<sub>2</sub>O<sub>2</sub> solution (100 ml, initial concentration = 1 mM), catalyst (0.10 g, 1 g·L<sup>-1</sup>), AM 1.5 filter, 25 °C.

The photocatalytic H<sub>2</sub>O<sub>2</sub> decomposition over different catalysts has been conducted with an initial H<sub>2</sub>O<sub>2</sub> concentration of 1 mM to investigate the decomposition behavior of H<sub>2</sub>O<sub>2</sub> in the presence of catalysts. As shown in Fig. S14A, the H<sub>2</sub>O<sub>2</sub> decomposes about 18% over g-C<sub>3</sub>N<sub>4</sub>-SiW<sub>11</sub> after 60 minutes, which is lower than those over g-C<sub>3</sub>N<sub>4</sub> (35%) and g-C<sub>3</sub>N<sub>4</sub>-SiW<sub>11</sub>-IMP (50%), but is a bit higher than that over K-SiW<sub>11</sub> (13%). The H<sub>2</sub>O<sub>2</sub> decomposes about 8% in the absence of catalyst. To more accurately evaluate the rate constants, we have fitted the decomposition data of different catalysts based on Eqn. S5 and presented in Fig. S14B, where  $K_d'$  is the first-order reaction rate constant.<sup>S3,S10</sup> The results in Table S3 indicates that the values of  $K_d'$  increases in the following order: None (0.0016 min<sup>-1</sup>) < K-SiW<sub>11</sub> (0.0023 min<sup>-1</sup>) < g-C<sub>3</sub>N<sub>4</sub>-SiW<sub>11</sub> (0.0033 min<sup>-1</sup>) < g-C<sub>3</sub>N<sub>4</sub> (0.0067 min<sup>-1</sup>) < g-C<sub>3</sub>N<sub>4</sub>-SiW<sub>11</sub>-IMP (0.0113 min<sup>-1</sup>).

$$-\frac{dc_t}{dt} = k_0 \quad (\text{Eqn. S5})$$

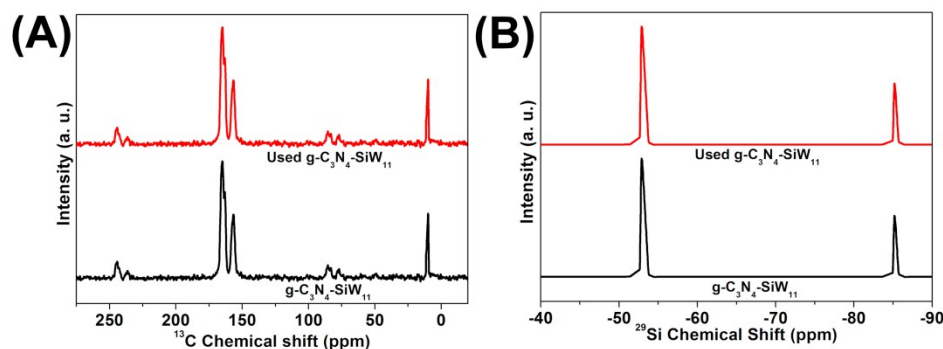


**Figure S15.** <sup>13</sup>C (A) and <sup>29</sup>Si (B) MAS NMR spectra of fresh and used g-C<sub>3</sub>N<sub>4</sub>-SiW<sub>11</sub>.

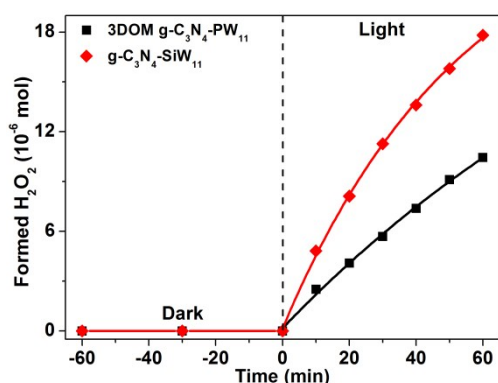


**Figure S16.** Photocatalytic  $\text{H}_2\text{O}_2$  production over 3DOM  $\text{g-C}_3\text{N}_4\text{-PW}_{11}$  and  $\text{g-C}_3\text{N}_4\text{-SiW}_{11}$  in the presence of methanol. Reaction conditions: methanol/water mixture (5/95 v/v, 100 ml), catalyst (0.10 g, 1 g·L<sup>-1</sup>),  $\text{O}_2$ -equilibrated, AM 1.5 filter, 25 °C.

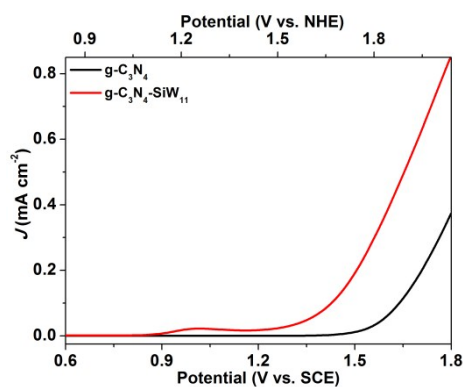


**Figure S17.** LSV curves of catalysts-loaded electrodes toward OER with scan rate of  $10 \text{ mV}\cdot\text{s}^{-1}$  in the dark.

The water oxidation performance has been evaluated by oxygen evolution reaction (OER).<sup>S10,S11</sup> Fig. S17 shows linear sweep voltammogram (LSV) curves of the electrodes with the  $\text{g-C}_3\text{N}_4$  and  $\text{g-C}_3\text{N}_4\text{-SiW}_{11}$  in the dark. The onset potential of  $\text{g-C}_3\text{N}_4$  is at approximately 1.71 V vs. normal hydrogen electrode (NHE) in the dark, which has a 0.48 V overpotential because the thermodynamic potential was 1.23 V vs. NHE. In addition, the slow increase of the current density ( $J$ ) with bias ( $E$ ) indicated a high kinetic barrier. In contrast, for  $\text{g-C}_3\text{N}_4\text{-SiW}_{11}$ , the onset potential negatively shifted to 1.49 V vs. NHE, and the current density was greatly enhanced compared to the  $\text{g-C}_3\text{N}_4$ . The above results reveal that the OER performance of  $\text{g-C}_3\text{N}_4\text{-SiW}_{11}$  is higher than that of  $\text{g-C}_3\text{N}_4$ .

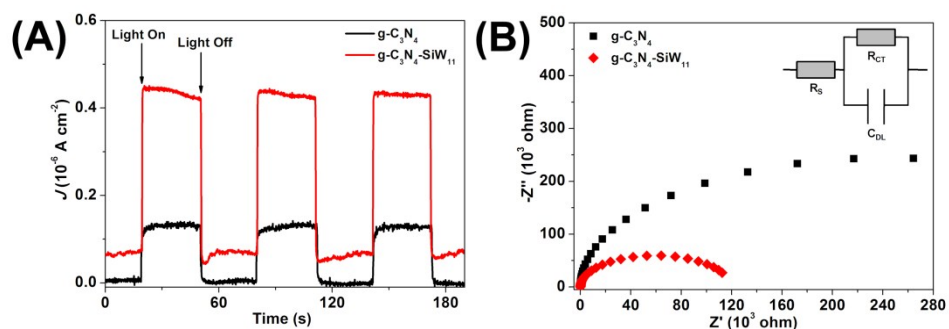


**Figure S18.** Photocurrent response of catalysts-loaded electrodes under sunlight (AM 1.5 filter) at a bias of 0.25 V vs. SCE (A); EIS Nyquist plots of the catalysts under sunlight (AM 1.5 filter) at a bias of 5 mV vs. SCE in the frequency range of 10 mHz to 100 kHz (B).

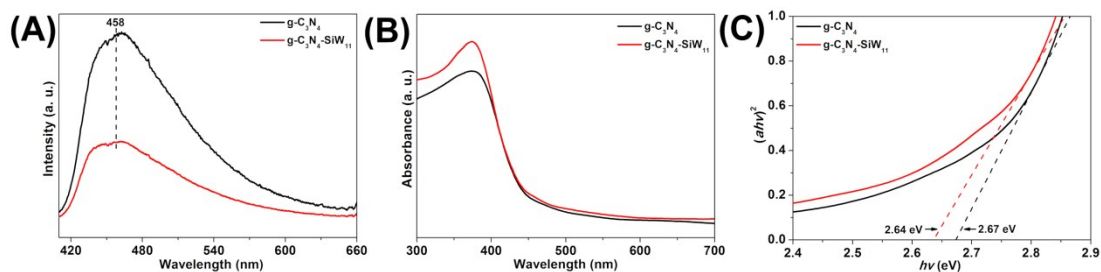


**Figure S19.** PL spectra (A), UV-DRS spectra (B), and Tauc plots of  $g\text{-C}_3\text{N}_4$  and  $g\text{-C}_3\text{N}_4\text{-SiW}_{11}$ .

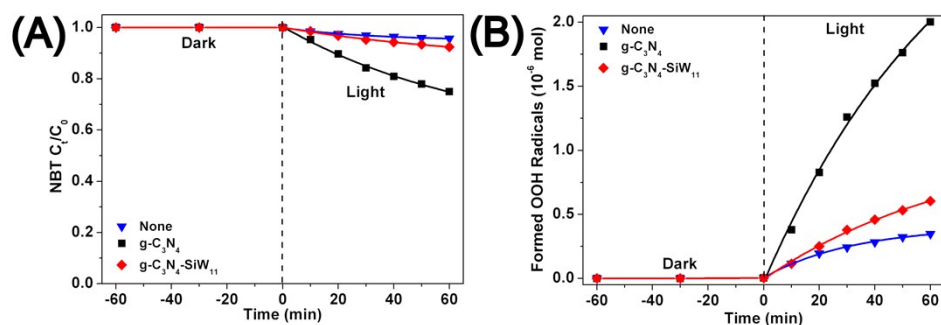


**Figure S20.** NBT decomposition (A) and  $\bullet\text{OOH}$  radicals formation (B) during the photoreaction over  $g\text{-C}_3\text{N}_4$  and  $g\text{-C}_3\text{N}_4\text{-SiW}_{11}$ .

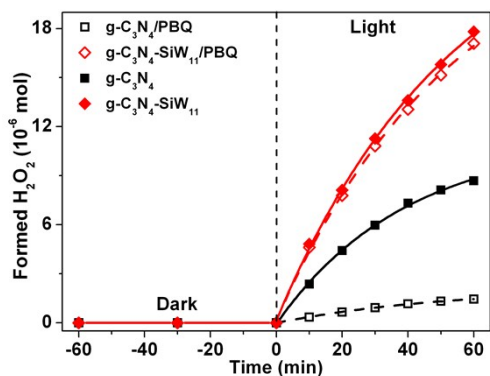


**Figure S21.** The effect of PBQ for the photocatalytic  $\text{H}_2\text{O}_2$  production over  $\text{g-C}_3\text{N}_4$  and  $\text{g-C}_3\text{N}_4\text{-SiW}_{11}$ .

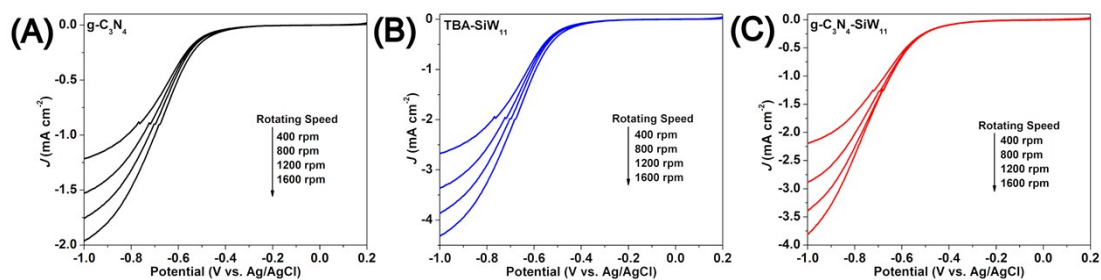


**Figure S22.** LSV curves of  $\text{g-C}_3\text{N}_4$  (A), TBA- $\text{SiW}_{11}$  (B) and  $\text{g-C}_3\text{N}_4\text{-SiW}_{11}$  (C) measured on RDE analysis at different rotating speeds.

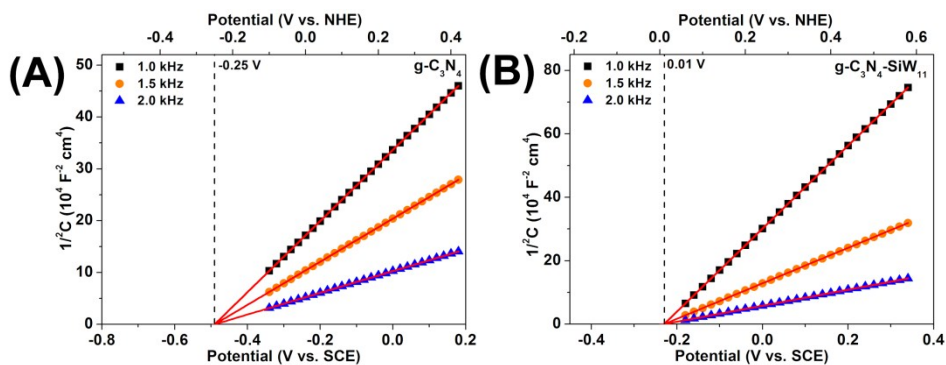


**Figure S23.** Mott-Schottky plots of  $\text{g-C}_3\text{N}_4$  (A) and  $\text{g-C}_3\text{N}_4\text{-SiW}_{11}$  (B) with frequency of 1.0 kHz, 1.5 kHz, and 2.0 kHz in the dark.

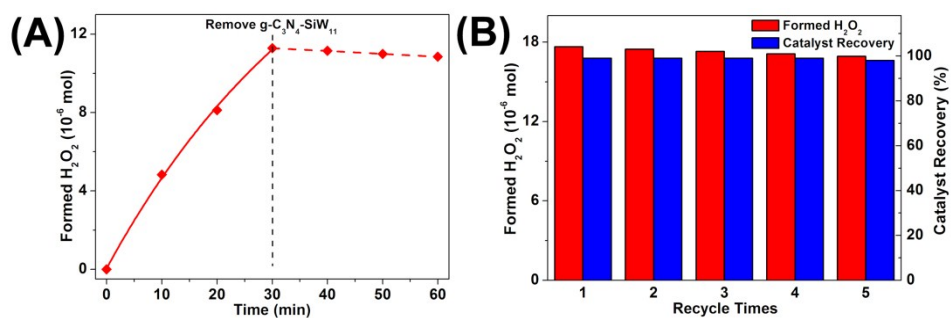


**Figure S24.** Experiment to prove the heterogeneous nature (A) and the recycle (B) of  $\text{g-C}_3\text{N}_4\text{-SiW}_{11}$ .

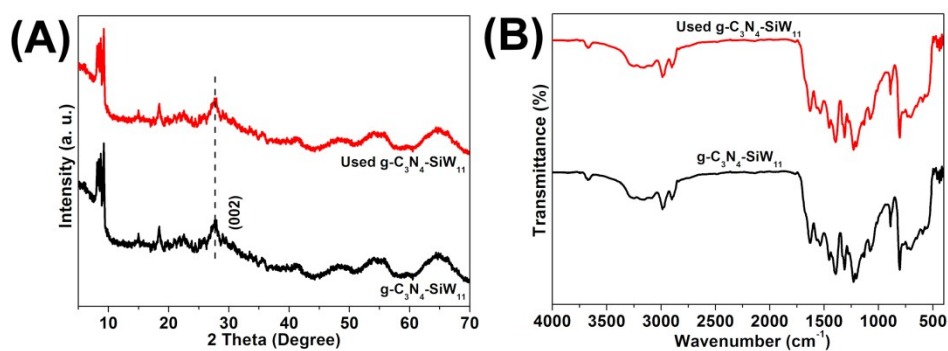


**Figure S25.** XRD patterns (A) and IR spectra (B) of fresh and used  $\text{g-C}_3\text{N}_4\text{-SiW}_{11}$ .

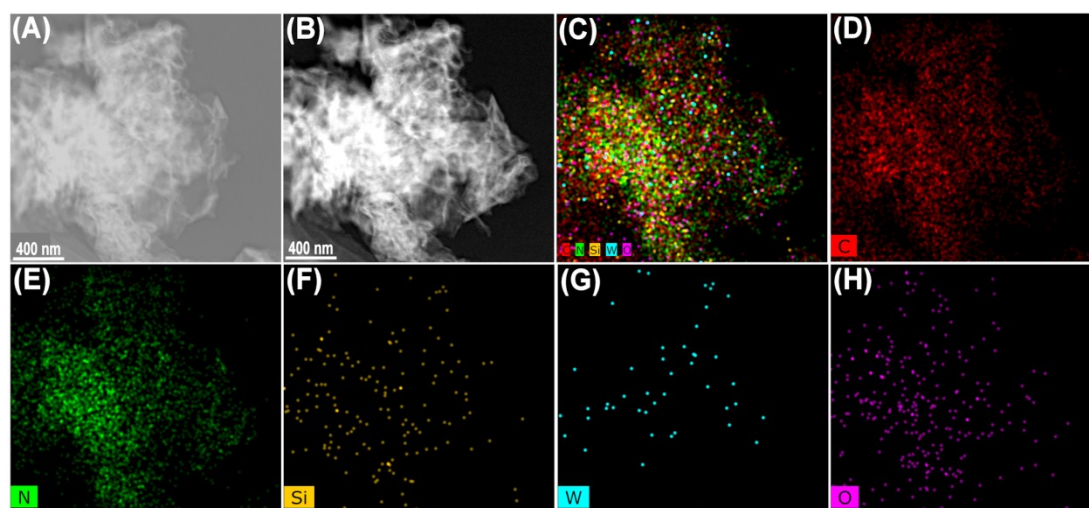


**Figure S26.** STEM images and corresponding elemental mappings of used  $\text{g-C}_3\text{N}_4\text{-SiW}_{11}$ .

It is essential to confirm the catalysis of  $g\text{-C}_3\text{N}_4\text{-SiW}_{11}$  is truly heterogeneous for photocatalytic  $\text{H}_2\text{O}_2$  production. When the reaction time arrives at 30 minute,  $g\text{-C}_3\text{N}_4\text{-SiW}_{11}$  has been removed from the reaction system by filtration, and the reaction is allowed to proceed with the filtrate under the same conditions. As shown in Fig. S23A, no new  $\text{H}_2\text{O}_2$  forms and the formed  $\text{H}_2\text{O}_2$  starts to decompose under the same conditions. Furthermore, the ICP-AES result reveals no W leaching in the filtrate. The above results rule out the contribution of W species leached into the reaction solution for the observed catalytic results and confirms the  $g\text{-C}_3\text{N}_4\text{-SiW}_{11}$  is truly heterogeneous for photocatalytic  $\text{H}_2\text{O}_2$  production.

To investigate the stability of heterogeneous  $g\text{-C}_3\text{N}_4\text{-SiW}_{11}$ , the photocatalytic  $\text{H}_2\text{O}_2$  production has been recycled for five times under the same conditions. Fig. S23B shows the catalytic performance is almost unchanged and the catalyst recovery can reach above 96% even after five times. The XRD, IR,  $^{13}\text{C}$  and  $^{29}\text{Si}$  MAS NMR results of the fresh and used  $g\text{-C}_3\text{N}_4\text{-SiW}_{11}$  exhibit almost the same typical peaks (Fig. S15 and S24). The STEM-Mapping results of the used  $g\text{-C}_3\text{N}_4\text{-SiW}_{11}$  (Fig. S25) indicate that the sheet-like structure and the dispersion of  $\text{SiW}_{11}$  cluster on  $g\text{-C}_3\text{N}_4\text{-SiW}_{11}$  are retained after reaction. The EA and ICP results in Table S2 also reveal that the composition of the used  $g\text{-C}_3\text{N}_4\text{-SiW}_{11}$  remains unchanged. The above results indicate that the heterogeneous  $g\text{-C}_3\text{N}_4\text{-SiW}_{11}$  is catalytic stable.

**Table S1.** Porous structural parameter for g-C<sub>3</sub>N<sub>4</sub> and g-C<sub>3</sub>N<sub>4</sub>-SiW<sub>11</sub>.

Catalyst	Surface Area (m <sup>2</sup> /g)	Pore Volume (cm <sup>3</sup> /g)	Pore Diameter (nm)
g-C <sub>3</sub> N <sub>4</sub>	57.5	0.235	3.6
g-C <sub>3</sub> N <sub>4</sub> -SiW <sub>11</sub>	66.1	0.351	3.8

**Table S2.** ICP and EA analysis of g-C<sub>3</sub>N<sub>4</sub> and g-C<sub>3</sub>N<sub>4</sub>-SiW<sub>11</sub>.

Catalyst	Found (wt.%)					
	C	N	H	K	Si	W
g-C <sub>3</sub> N <sub>4</sub> (C <sub>2.61</sub> N <sub>4</sub> H <sub>1.58</sub> )	35.24	62.98	1.59	-	-	-
g-C <sub>3</sub> N <sub>4</sub> -SiW <sub>11</sub> (C <sub>2.61</sub> N <sub>4</sub> H <sub>1.55</sub> (K <sub>4</sub> SiW <sub>11</sub> O <sub>42</sub> Si <sub>2</sub> C <sub>8</sub> H <sub>14</sub> N <sub>2</sub> ) <sub>0.007</sub> )	28.99	50.90	1.50	0.99	0.53	12.82
Used g-C <sub>3</sub> N <sub>4</sub> -SiW <sub>11</sub> (C <sub>2.61</sub> N <sub>4</sub> H <sub>1.55</sub> (K <sub>4</sub> SiW <sub>11</sub> O <sub>42</sub> Si <sub>2</sub> C <sub>8</sub> H <sub>14</sub> N <sub>2</sub> ) <sub>0.007</sub> )	28.99	50.90	1.50	0.99	0.53	12.82

**Table S3.** Products distribution for photocatalytic H<sub>2</sub>O<sub>2</sub> production over different catalysts in 60 minutes.

Catalyst	H <sub>2</sub> O <sub>2</sub> <sup>b</sup> (μmol)	HCHO <sup>b</sup> (μmol)	HCOOH <sup>b</sup> (μmol)	CO <sub>2</sub> <sup>b</sup> (μmol)	H <sub>2</sub> O <sub>2</sub> Selectivity <sup>c</sup> (%)
g-C <sub>3</sub> N <sub>4</sub> -SiW <sub>11</sub>	17.8	21.4	0.1	1.5	80.1
g-C <sub>3</sub> N <sub>4</sub> -SiW <sub>11</sub> - IMP	9.6	41.5	0.3	2.9	22.2
g-C <sub>3</sub> N <sub>4</sub>	8.7	9.3	0.2	1.1	86.6
K-SiW <sub>11</sub>	1.0	32.8	0.1	1.9	3.0
None	<0.1	<0.1	<0.1	<0.1	<0.1

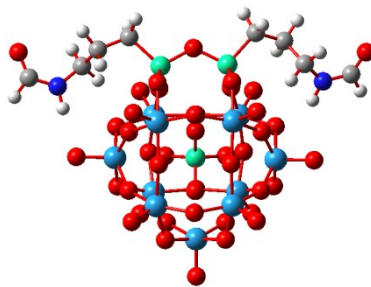
<sup>a</sup> Reaction conditions: methanol/water mixture (5/95 v/v, 100 ml), catalyst (0.10 g, 1 g·L<sup>-1</sup>), O<sub>2</sub>-equilibrated, AM 1.5 filter, 25 °C, 60 minutes; <sup>b</sup> Formed H<sub>2</sub>O<sub>2</sub> (μmol), HCHO (μmol), HCOOH (μmol) and CO<sub>2</sub> (μmol) were obtained from the photoreaction mixture at 60 minute. <sup>c</sup> H<sub>2</sub>O<sub>2</sub> Selectivity = [H<sub>2</sub>O<sub>2</sub>]/([HCHO] + [HCOOH] + [CO<sub>2</sub>]/2) × 100

**Table S4.** Rate constants for photocatalytic H<sub>2</sub>O<sub>2</sub> formation and decomposition over different catalysts.<sup>a</sup>

Catalyst	Maximum Formed H <sub>2</sub> O <sub>2</sub> <sup>b</sup> (μmol)	H <sub>2</sub> O <sub>2</sub> Formation Rate <sup>b</sup> (μmol·h <sup>-1</sup> )	K <sub>f</sub> <sup>c</sup> (μmol·min <sup>-1</sup> )	K <sub>d</sub> <sup>c</sup> (min <sup>-1</sup> )	K <sub>d</sub> <sup>d</sup> (min <sup>-1</sup> )
g-C <sub>3</sub> N <sub>4</sub> -SiW <sub>11</sub>	91.4	15.2	0.4831	0.0183	0.0033
g-C <sub>3</sub> N <sub>4</sub> -SiW <sub>11</sub> - IMP	24.0	4.0	0.2981	0.0232	0.0113
g-C <sub>3</sub> N <sub>4</sub>	19.1	3.2	0.2862	0.0254	0.0067
K-SiW <sub>11</sub>	3.7	0.6	0.0255	0.0163	0.0023
None	<0.1	<0.1	0.0027	0.0093	0.0016

<sup>a</sup> Reaction conditions: methanol/water mixture (5/95 v/v, 100 ml), catalyst (0.10 g, 1 g·L<sup>-1</sup>), O<sub>2</sub>-equilibrated, AM 1.5 filter, 25 °C; <sup>b</sup> Maximum formed H<sub>2</sub>O<sub>2</sub> (μmol) and H<sub>2</sub>O<sub>2</sub> formation rate (μmol·h<sup>-1</sup>) were obtained from Fig. 3C; <sup>c</sup> K<sub>f</sub> and K<sub>d</sub> values were estimated by fitting the photocatalytic H<sub>2</sub>O<sub>2</sub> formation data according to Eqn. 5; <sup>d</sup> K<sub>d</sub> values were estimated by fitting the photocatalytic H<sub>2</sub>O<sub>2</sub> decomposition data according to Eqn. S4.

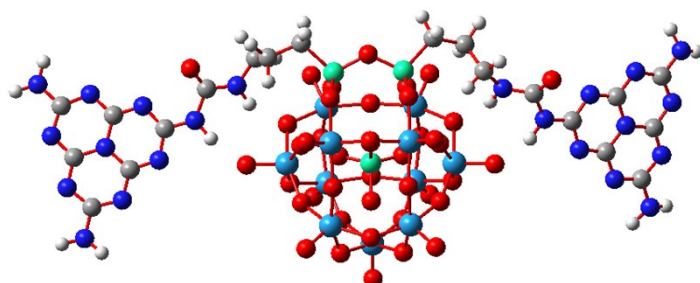
**Table S5.** Cartesian coordinates for the models for SiW<sub>11</sub>-organic linker.



C	-2.98281762	5.13080337	0.62849673	O	-3.01592822	0.84404575	1.13116342
H	-2.74460487	5.85083735	1.42470723	O	-1.81182539	2.97044721	2.02823278
H	-2.9660138	5.69842907	-0.31371715	O	1.48091333	3.0328375	2.2407749
C	-4.38990866	4.53576965	0.88337931	O	3.62467148	1.35676264	-0.99604751
H	-4.32041159	3.76696295	1.66093518	O	2.35545735	0.4125421	-3.1481455
H	-5.0789881	5.30525688	1.26116616	O	-1.82956331	0.37404667	-3.46365287
C	-5.00814974	3.90910966	-0.38083099	O	-3.39390275	1.32742996	-1.55481467
H	-4.25651618	3.34306547	-0.93161962	O	-0.13395352	4.64532606	0.78336286
H	-5.39676967	4.69496595	-1.03867932	O	1.61534054	3.02647375	-0.49163352
C	2.6234238	5.34401647	0.89912612	O	2.77154347	3.12191322	-3.01241753
H	2.12328426	6.22278091	0.46866818	O	0.21009926	1.97562976	-2.50122176
H	2.84408247	5.59582916	1.9471585	O	-2.21506381	3.09534078	-3.43282748
C	3.92397988	5.06409928	0.11967071	O	-1.55551241	2.97104368	-0.72680858
H	3.66863053	4.72631264	-0.89019412	O	-0.03481885	-1.70518193	0.68127361
H	4.52207216	5.98095489	0.00252721	O	-0.0747021	0.91220939	1.28162051
C	4.80397077	3.98527556	0.78313131	O	1.42526418	0.00745291	-0.77953573
H	4.17890098	3.21505161	1.24303166	O	-1.26554256	-0.00211069	-0.97627818
H	5.42942821	4.42413185	1.56715405	Si	-1.58958802	3.8469874	0.6550565
O	-2.99616223	-3.31876647	2.98165211	Si	1.36461225	3.9222294	0.85995483
O	-0.22049683	-2.89362612	2.9700285	W	-1.85899732	-2.5054582	1.98130859
O	2.50247605	-3.2832306	3.45716429	W	1.51671635	-2.48128531	2.29932251
O	1.29254016	-3.89332984	0.99821636	W	0.08964055	-3.74379749	-0.4969335
O	0.14084832	-5.35408777	-1.09787875	W	-1.85271509	1.15478726	2.7029401
O	-1.36826876	-3.91132105	0.7800983	W	1.49616237	1.20249455	2.89841273
O	-1.79328365	-0.73861127	2.79024561	W	3.57214515	-0.23076954	0.17046682
O	1.39329264	-0.70566521	3.03289485	W	2.06199623	-1.43091605	-2.62720537
O	2.85778687	-1.70574162	1.12487091	W	-1.65444751	-1.46935849	-2.8656305
O	1.45221076	-2.89228907	-1.53140463	W	-3.53630393	-0.16207086	-0.36143846
O	-1.14651715	-2.90725269	-1.71504791	W	2.07580815	1.91874292	-1.99908378
O	-2.98843509	-1.71251699	0.6734309	W	-1.68405951	1.89544926	-2.32092655
O	-3.00957102	1.43654041	3.94658199	Si	0.01115451	-0.16663187	0.06272656
O	-0.25202717	1.40909452	3.7185285	N	5.67811004	3.30192039	-0.1641498
O	2.44660161	1.50620864	4.30103946	H	5.25310008	2.51023652	-0.65087622
O	2.85555426	0.86699777	1.56032496	N	-6.10010079	2.97407305	-0.10395284
O	5.24173957	-0.28626709	0.58392891	H	-5.86741198	1.98264561	-0.05499749
O	3.58473451	-1.26172116	-1.46104411	C	-7.38611861	3.33116333	0.04919596
O	2.77437168	-2.25156219	-3.95831729	O	-7.85269573	4.47112081	-0.00447141
O	0.24679181	-1.2709634	-3.17158538	C	6.94426704	3.65840438	-0.43319456

O	-2.15686979	-2.30063731	-4.28293589	O	7.57385356	4.59760324	0.0603456
O	-3.31069102	-1.28657227	-1.94742738	H	-8.03338806	2.44593612	0.23196858
O	-5.25824964	-0.1550496	-0.17966858	H	7.4041108	2.98157278	-1.18482124

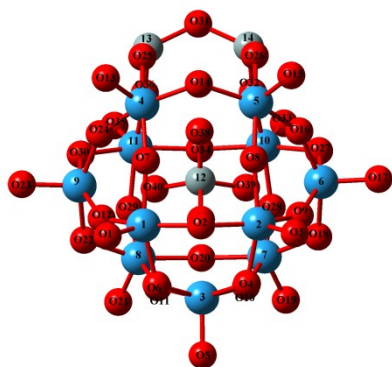
**Table S6.** Cartesian coordinates for the models for g-C<sub>3</sub>N<sub>4</sub>-SiW<sub>11</sub>.



C	-2.84467503	4.92216724	1.69711177	W	1.482308	-2.98399	2.059495
H	-2.74301869	5.30083513	2.72388538	W	0.023408	-3.7298	-0.9042
H	-2.66276092	5.78027495	1.03365964	W	-1.83701	0.610983	3.05792
C	-4.27173016	4.36013234	1.48506775	W	1.510148	0.551426	3.26472
H	-4.3189985	3.33285884	1.86368852	W	3.559387	-0.4446	0.325246
H	-5.01003429	4.93201341	2.06300533	W	2.038542	-1.13743	-2.63025
C	-4.69579287	4.36017222	-0.00303569	W	-1.67474	-1.06828	-2.86856
H	-3.81408913	4.321808	-0.64551684	W	-3.52996	-0.19404	-0.16523
H	-5.24805152	5.27553679	-0.24195432	W	2.113342	2.065151	-1.45213
C	2.76146318	4.92193396	1.94051431	W	-1.64765	2.157509	-1.75521
H	2.35710943	5.8371731	1.48648998	Si	0.010636	-0.29709	0.247232
H	2.87041495	5.1313969	3.0151392	N	5.692494	2.661812	1.098142
C	4.12855787	4.59782672	1.30443755	H	5.181243	2.128397	0.390363
H	3.97162057	4.33001491	0.25441396	N	-5.51626	3.215309	-0.38855
H	4.7834194	5.48273795	1.30179031	H	-4.98901	2.415099	-0.74798
C	4.85349351	3.43516455	2.01056802	C	-6.8229	3.132198	-0.07729
H	4.12278949	2.74565333	2.44643483	O	-7.50999	4.021401	0.404065
H	5.49545482	3.79561192	2.81806004	C	6.988927	2.394971	1.338813
O	-3.03958099	-3.8365654	2.6201692	O	7.720046	2.936683	2.154173
O	-0.26180937	-3.46848049	2.66682858	N	-7.35129	1.808288	-0.35563
O	2.45437732	-3.97879886	3.06509375	C	-8.63099	1.50613	-0.616
O	1.23061309	-4.14376021	0.54486303	H	-6.71007	1.004217	-0.23732
O	0.0475894	-5.2180634	-1.76014576	N	-8.92728	0.177867	-0.58484
O	-1.42816276	-4.08261088	0.34087352	N	-9.50727	2.49947	-0.91568
O	-1.80445504	-1.276838	2.8308176	C	-10.1685	-0.17885	-0.80976
O	1.38473267	-1.34914259	3.0704354	C	-10.7554	2.160722	-1.13382
O	2.85177499	-2.0447208	1.02891372	N	-11.1542	0.804211	-1.07682
O	1.40574093	-2.74478938	-1.78533091	N	-10.5467	-1.46692	-0.77833
O	-1.19370246	-2.68178418	-1.95992775	N	-11.6915	3.086694	-1.41508
O	-3.01483196	-1.88160957	0.59071228	C	-12.496	0.436703	-1.27497
O	-2.98291265	0.69921577	4.33666004	C	-11.837	-1.71767	-0.97976
O	-0.22927854	0.65340615	4.10339581	C	-12.9345	2.643783	-1.58692
O	2.4737679	0.59805203	4.68806726	N	-12.8449	-0.84506	-1.21241
O	2.86124383	0.42028669	1.86969582	N	-13.4051	1.382244	-1.52153
O	5.25059762	-0.54237187	0.70607621	N	-12.1984	-3.03564	-0.9732

O	3.56261312	-1.1827485	-1.44870107	N	-13.8726	3.599682	-1.89558
O	2.74150001	-1.73491411	-4.07666707	H	-13.1802	-3.23598	-0.85911
O	0.22977027	-0.86135349	-3.13967403	H	-11.5223	-3.67933	-0.58771
O	-2.18732883	-1.6448077	-4.40079966	H	-14.8317	3.334307	-1.7248
O	-3.32480963	-1.01386238	-1.92683017	H	-13.6036	4.547515	-1.6719
O	-5.26014644	-0.17553966	-0.02207023	N	7.449627	1.285738	0.516436
O	-3.00994558	0.56633249	1.46630064	C	8.661201	1.166232	-0.03422
O	-1.76246286	2.50878339	2.69223328	H	6.813721	0.472565	0.458403
O	1.548273	2.46596938	2.92395177	N	8.956903	-0.06282	-0.54002
O	3.6492825	1.31974444	-0.55489201	N	9.472701	2.255351	-0.08257
O	2.35946779	0.76580425	-2.83196501	C	10.11068	-0.21308	-1.14405
O	-1.81518054	0.85125317	-3.13721997	C	10.63284	2.11939	-0.67795
O	-3.37601042	1.49326121	-1.09177182	N	11.01104	0.877171	-1.24238
O	-0.02298448	4.32978528	1.75800267	N	10.4744	-1.38943	-1.68093
O	1.66421924	2.89331849	0.22445169	N	11.48991	3.152244	-0.78335
O	2.8241383	3.41226133	-2.24603249	C	12.23872	0.73273	-1.91086
O	0.2413646	2.24172396	-1.92583776	C	11.6542	-1.42956	-2.29243
O	-2.17847776	3.52805332	-2.64699433	C	12.6304	2.917364	-1.42668
O	-1.5094057	2.97651245	-0.01405955	N	12.56307	-0.44055	-2.44786
O	-0.05959931	-1.91331686	0.60372246	N	13.06287	1.777656	-2.00282
O	-0.06029495	0.57863376	1.6195233	N	12.015	-2.64156	-2.81948
O	1.43155827	-0.01841557	-0.55732181	N	13.50615	3.974715	-1.49839
O	-1.26707991	0.05846444	-0.74544401	H	12.73569	-2.61544	-3.52582
Si	-1.49929956	3.60947011	1.49672345	H	11.25646	-3.29761	-2.94585
Si	1.4542285	3.56795109	1.70362537	H	14.19799	3.909451	-2.23124
W	-1.88644366	-2.89444369	1.76667624	H	13.08857	4.880469	-1.3355

**Table S7.** Mulliken charge distribution on O atoms of SiW<sub>11</sub>-organic linker and g-C<sub>3</sub>N<sub>4</sub>-SiW<sub>11</sub> by DFT method.



Atom	Charge	Atom	Charge	Atom	Charge	Atom	Charge
1: 30.07  e							
O1	-0.58	O11	-0.84	O21	-0.58	O31	-0.67
O2	-0.79	O12	-0.84	O22	-0.79	O32	-0.80
O3	-0.58	O13	-0.57	O23	-0.67	O33	-0.58
O4	-0.79	O14	-0.81	O24	-0.85	O34	-0.86

O5	-0.58	O15	-0.57	O25	-0.76	O35	-0.58
O6	-0.79	O16	-0.85	O26	-0.76	O36	-0.79
O7	-0.83	O17	-0.59	O27	-0.85	O37	-0.86
O8	-0.83	O18	-0.80	O28	-0.79	O38	-0.83
O9	-0.84	O19	-0.58	O29	-0.79	O39	-0.85
O10	-0.84	O20	-0.84	O30	-0.82	O40	-0.85
<b>Atom</b>	<b>Charge</b>	<b>Atom</b>	<b>Charge</b>	<b>Atom</b>	<b>Charge</b>	<b>Atom</b>	<b>Charge</b>
2: 29.77  e							
O1	-0.59	O11	-0.84	O21	-0.59	O31	-0.61
O2	-0.79	O12	-0.84	O22	-0.80	O32	-0.75
O3	-0.59	O13	-0.58	O23	-0.59	O33	-0.59
O4	-0.79	O14	-0.81	O24	-0.84	O34	-0.86
O5	-0.59	O15	-0.58	O25	-0.73	O35	-0.59
O6	-0.80	O16	-0.84	O26	-0.73	O36	-0.75
O7	-0.83	O17	-0.59	O27	-0.79	O37	-0.85
O8	-0.82	O18	-0.80	O28	-0.79	O38	-0.83
O9	-0.84	O19	-0.59	O29	-0.79	O39	-0.85
O10	-0.84	O20	-0.84	O30	-0.79	O40	-0.85

## References

- S1 a) R. Villanneau, A. Marzouk, Y. Wang, A. B. Djamaa, G. Laugel, A. Proust and F. Launay, *Inorg. Chem.*, 2013, **52**, 2958-2965; b) Y. Ji, J. Hu, L. Huang, W. Chen, C. Streb and Y. F. Song, *Chem. Eur. J.*, 2015, **21**, 6469-6474.
- S2 a) Y. Zheng, L. Lin, B. Wang and X. Wang, *Angew. Chem.*, 2015, **127**, 13060-13077; *Angew. Chem. Int. Ed.*, 2015, **54**, 12868-12884; b) W. J. Ong, L. L. Tan, Y. H. Ng, S. T. Yong and S. P. Chai, *Chem. Rev.*, 2016, **116**, 7159-7329.
- S3 Y. Kofuji, Y. Isobe, Y. Shiraishi, H. Sakamoto, S. Tanaka, S. Ichikawa and T. Hirai, *J. Am. Chem. Soc.*, 2016, **138**, 10019-10025.
- S4 Y. Liu, H. Liu, C. Wang, S. X. Hou and N. Yang, *Environ. Sci. Technol.*, 2013, **47**, 13889-13895.
- S5 a) S. Obregón, Y. Zhang and G. Colón, *Appl. Catal. B: Environ.*, 2016, **184**, 96-103; b) Z. Wei, D. Liu, W. Wei, X. Chen, Q. Han, W. Yao, X. Ma and Y. Zhu, *ACS Appl. Mater. Interfaces*, 2017, **9**, 15533-15540.
- S6 P. Hohenberg and W. Kohn, *Phys. Rev.*, 1964, **136**, B864-B871.
- S7 P. J. Stephens, F. J. Devlin, C. F. Chabalowski and M. J. Frisch, *J. Phys. Chem.*, 1994, **98**, 11623-11627.
- S8 a) P. J. Hay and W. R. Wadt, *J. Chem. Phys.*, 1985, **82**, 270-283; b) W. R. Wadt and P. J. Hay, *J. Chem. Phys.*, 1985, **82**, 284-298; c) P. J. Hay and W. R. Wadt, *J. Chem. Phys.*, 1985, **82**, 299-310.
- S9 M. J. Frisch, G. W. Trucks, H. B. Schlegel, G. E. Scuseria, M. A. Robb, J. R. Cheeseman, G. Scalmani, V. Barone, B. Mennucci, G. A. Petersson, H. Nakatsuji, M. Caricato, X. Li, H. P. Hratchian, A. F. Izmaylov, J. Bloino, G. Zheng, J. L. Sonnenberg, M. Hada, M. Ehara, K. Toyota, R. Fukuda, J. Hasegawa, M. Ishida, T. Nakajima, Y. Honda, O. Kitao, H. Nakai, T. Vreven, J. A. Montgomery Jr., J. E. Peralta, F. Ogliaro, M. Bearpark, J. J. Heyd, E. Brothers, K. N. Kudin, V. N. Staroverov, T. Keith, R. Kobayashi, J. Normand, K. Raghavachari, A. Rendell, J. C. Burant, S. S. Iyengar, J. Tomasi, M. Cossi, N. Rega, J. M. Millam, M. J. Klene, E. Knox, J. B. Cross, V. Bakken, C. Adamo, J. Jaramillo, R. Gomperts, R. E. Stratmann, O. Yazyev, A. J. Austin, R. Cammi, C. Pomelli, J. W. Ochterski, R. L. Martin, K. Morokuma, V. G. Zakrzewski, G. A. Voth, P. Salvador, J. J. Dannenberg, S. Dapprich, A. D. Daniels, O. Farkas, J. B. Foresman, J. V. Ortiz, J. Cioslowski and D. J. Fox, GAUSSIAN 09 (Revision B.01), Gaussian, Inc., Wallingford, CT, 2010.
- S10 R. Wang, K. Pan, D. Han, J. Jiang, C. Xiang, Z. Huang, L. Zhang and X. Xiang, *ChemSusChem*, 2016, **9**, 2470-2479.
- S11 G. H. Moon, M. Fujitsuka, S. Kim, T. Majima, X. Wang and W. Choi, *ACS Catal.*, 2017, **7**, 2886-2895.

